Electronic Supplementary Information

Shape-Persistent Porous Organic Cage Supported Palladium Nanoparticles as Heterogeneous Catalytic Materials

Shan Jiang,*[a] Harrison J. Cox,[a] Evangelos I. Papaioannou,[b] Chenyang Tang,[b] Huiyu Liu,[a] Billy Murdoch,[c†] Emma K. Gibson,[de] Ian S. Metcalfe,[b] John S. O. Evans,[a] Simon K. Beaumont*[a]

[a] *Department of Chemistry, Science Site, Durham University, South Road, Durham DH1 3LE, United Kingdom. E-mail (S.J.): shan.jiang@durham.ac.uk (S.K.B.): simon.beaumont@durham.ac.uk*
[b] *School of Engineering, Newcastle University, Newcastle-upon-Tyne, NE1 7RU, United Kingdom.*
[c] *National EPSRC XPS Users' Service (NEXUS), School of Engineering, Newcastle University, Newcastle upon Tyne, NE1 7RU, United Kingdom.*
[d] *School of Chemistry, University of Glasgow, University Avenue, Glasgow, G12 8QQ, United Kingdom.*
[e] *UK Catalysis Hub, Research Complex at Harwell, Oxfordshire, OX11 0FA, United Kingdom.*

This file contains:

Table S1. Synthesis of **$Pd(NO_3)_2$@CC3** crystals with various nominal Pd loadings

	Mass of **CC3**	Volume of $Pd(NO_3)_2$ stock solution used for **$Pd(NO_3)_2$@CC3** cocrystals (3 mg/ml)
1 wt.% $Pd(NO_3)_2$ loading	10 mg	30 µL
2 wt.% $Pd(NO_3)_2$ loading	10 mg	60 µL
4 wt.% $Pd(NO_3)_2$ loading	10 mg	120 µL
8 wt.% $Pd(NO_3)_2$ loading	10 mg	240 µL

Table S2. Pd loadings verified by ICP-OES

$Pd(NO_3)_2$ loading (wt.% $Pd(NO_3)_2$)	Expected / calculated wt.% Pd based on precursor amount.	Wt.% Pd obtained from ICP-OES data.
1	0.46	0.5
2	0.92	1
4	1.8	2
8	3.7	4

X-ray Absorption Spectroscopy (XAS) – further details of processing methods.

XANES spectra were aligned by calibration of the first zero crossing point of the second derivative of the Pd foil reference spectra in each case. XAFS data processing was performed using IFEFFIT[1] with the Horae package[2] (Athena and Artemis). The amplitude reduction factor,

S_0^2 was derived from EXAFS data analysis of the Pd foil reference spectrum (for which the co-ordination numbers of the fcc metal are known), yielding a value of 0.87±0.04. This was then fixed in the analysis of sample spectra. The parameters corresponding to the correction to the photoelectron energy origin, co-ordination numbers, bond lengths, and mean-squared relative deviation of atoms around absorbing atoms were then varied during fitting. Two small heteroatom environments (based on nearest neighbour oxygen and nitrogen in crystalline $Pd(NO_3)_2$[3]) and the Pd-Pd nearest neighbour distance in fcc metal were considered as possible contributions for first shell fits. The number of variables was kept to a minimum by making the physically reasonable assumption that the mean-squared relative deviation of the two small heteroatom neighbours is the same (the primary conclusion of the fits in which this is the case is that there is no significant contribution from Pd-Pd interactions). These fits are shown in Figure S7 and Table S4. All fits were performed using multiple k-weight fitting, although k^3-weighted data is shown in figures. Improved fits of the reference metal foil (Figure S8, Table S5) and the sample treated at 200 °C containing small nanoparticles (Figure S9, Table S5) were obtained by fitting to higher values of R using a model accounting for multiple scattering paths (those regarded significant in Feff) up to 5 Å effective path length, and using the further physically reasonable assumption that all Pd-Pd interactions grow or shrink by a constant scaling factor relative to the known bulk Pd fcc metal crystal. Assumed relations of co-ordination number and mean-squared relative deviation are tabulated in Table S3.

Table S3. Assumed relations of co-ordination number and mean-squared relative deviation used in extended Pd fits (based on fcc structure).

Scattering path	Co-ordination number	σ^2
Pd1 Single scattering	*12*	σ^2(Pd1)
Pd2 Single scattering	*6*	σ^2(Pd2)
Pd1Pd1 Acute triangle	*48*[a]	2 × σ^2(Pd1)
Pd1Pd2 Other double scattering	*48*	σ^2(Pd1)+ σ^2(Pd2)
Pd 3 Single scattering	*24*	σ^2(Pd3)
Pd1Pd1 Obtuse triangle	*48*[a]	2 × σ^2(Pd1)
Pd1Pd3 Obtuse triangle	*96*	σ^2(Pd1)+ σ^2(Pd3)
Pd4 Single scattering	*12*	σ^2(Pd4)
Pd1Pd1 Non-forward linear	*12*[a]	2 × σ^2(Pd1)
Pd1Pd4 Forward scattering	*24*	σ^2(Pd4)
Pd1 Forward through absorber	*12*	2 × σ^2(Pd1)
Pd1Pd4Pd1 Double forward scattering	*12*	σ^2(Pd4)

[a]To minimise the number of independent parameters the approximation is made that $CN_{Pd1xPd1}$ can be used when fitting all three of these paths involving two nearest shell Pd scatterers and the 4:4:1 ratio maintained.

Additional data and characterization results

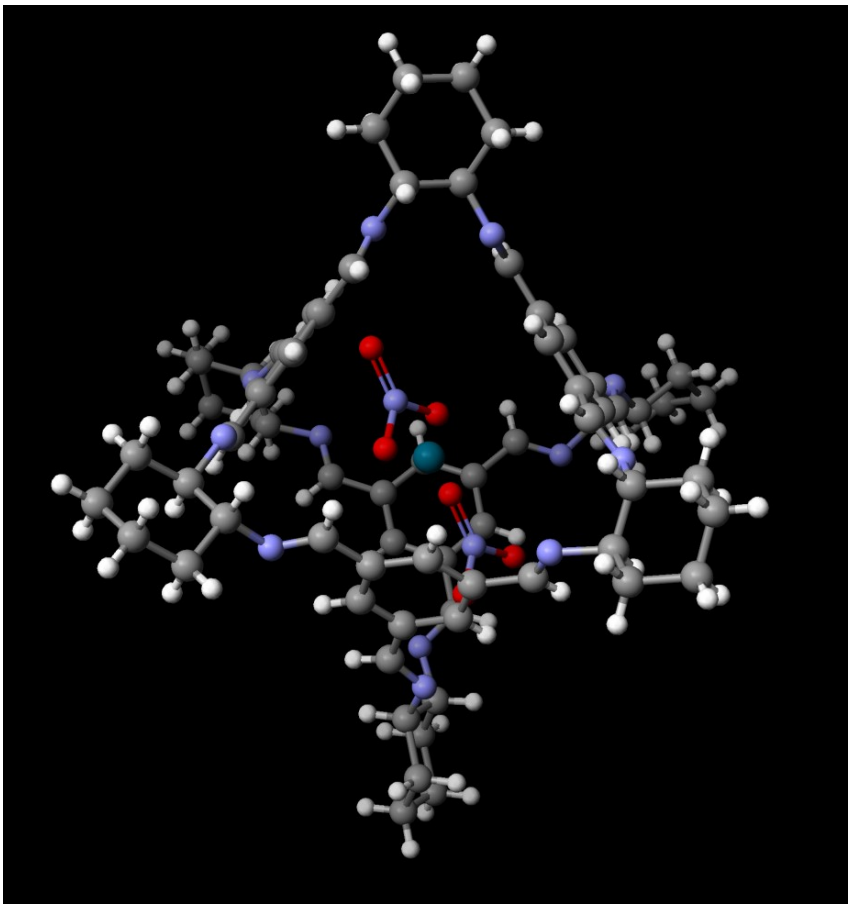

Figure S1. A structural model of $Pd(NO_3)_2$ fitting inside **CC3**.

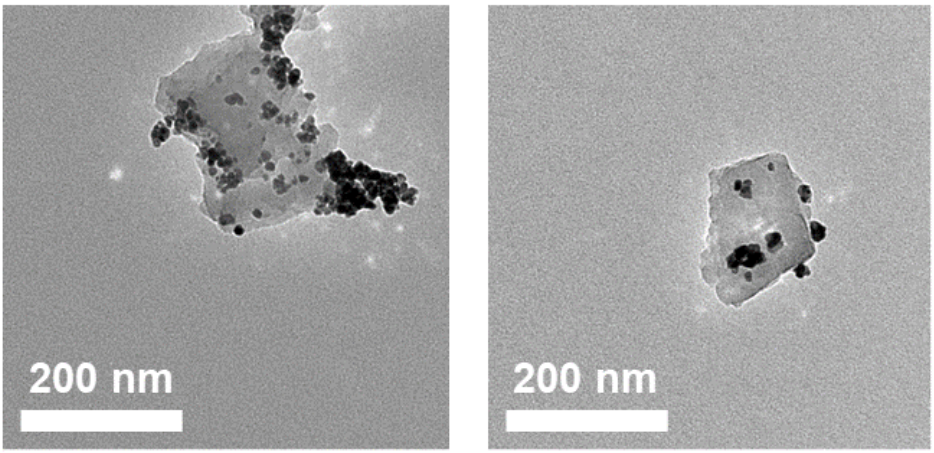

Figure S2. TEM images of **Pd NPs / CC3** produced from $Pd(acac)_2$ showing much lower degree of particle size control obtained.

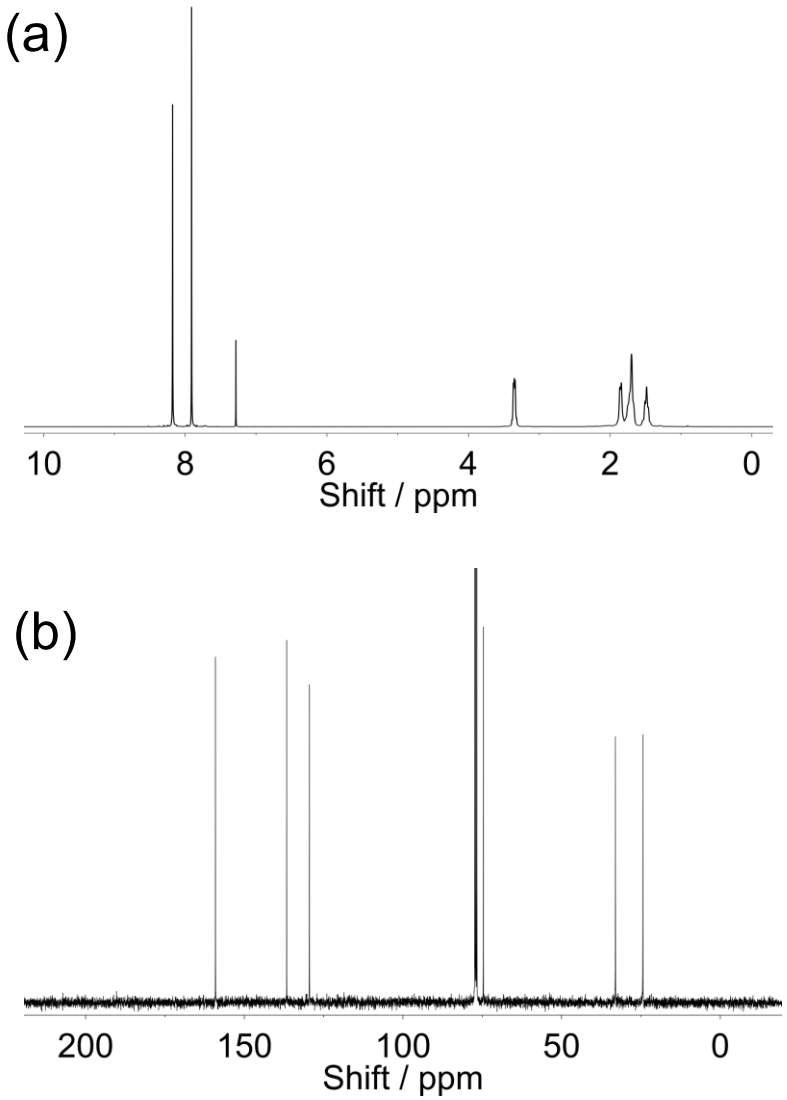

Figure S3. (a) ^{1}H NMR spectrum ($CDCl_3$) of **CC3**-*R*. (b) ^{13}C NMR spectrum ($CDCl_3$) of **CC3**-*R*.

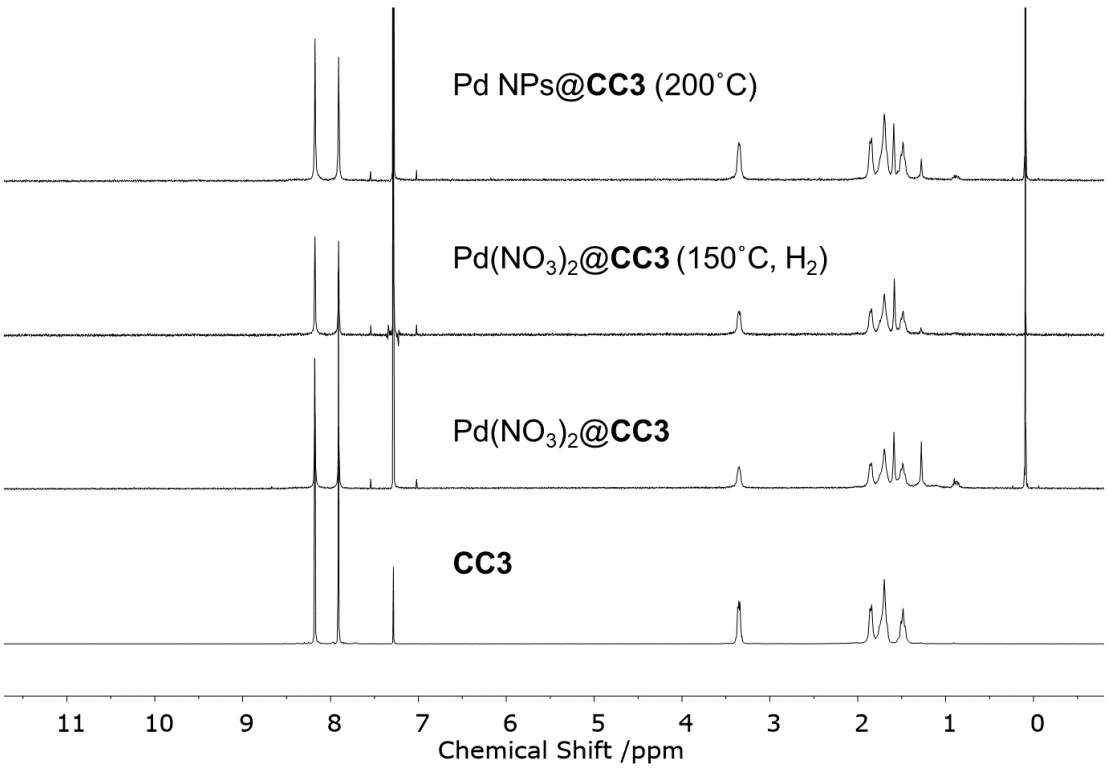

Figure S4. ^{1}H NMR spectra for pure **CC3**, 0.5 wt.% **Pd(NO$_3$)$_2$@CC3**, this sample after H_2 reduction at 150 ˚C for 1 hour, and 0.5 wt.% **Pd NPs@CC3** (the sample formed after H_2 reduction at 200 ˚C for 1 hour). It should be noted peaks at 0.88 and 1.26, and 1.56 ppm are due to contaminants during processing (silicone grease, grease and water respectively), and so no discernible changes are seen in the spectra obtained.

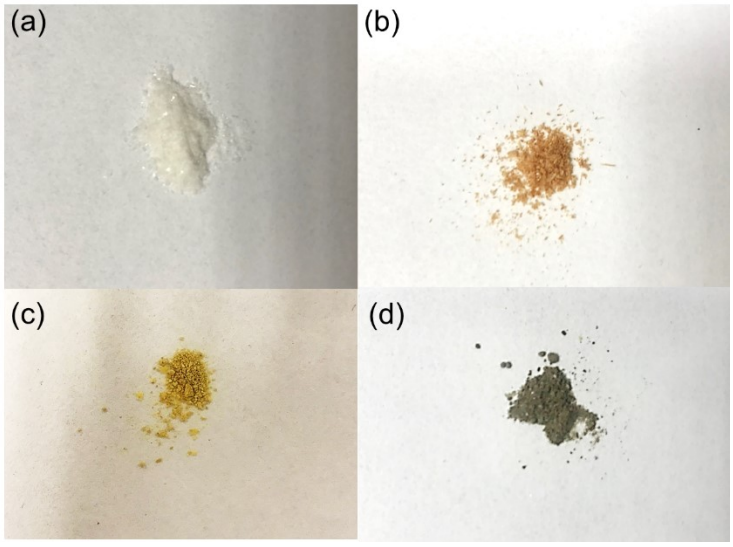

Figure S5. Photographs showing the relative colours of (a) **CC3**; (b) **Pd(NO$_3$)$_2$@CC3** as prepared; (c) **Pd(NO$_3$)$_2$@CC3** after reduction at 150 °C and (d) **Pd(NO$_3$)$_2$@CC3** after reduction at 200 °C (referred to as **PdNP@CC3**).

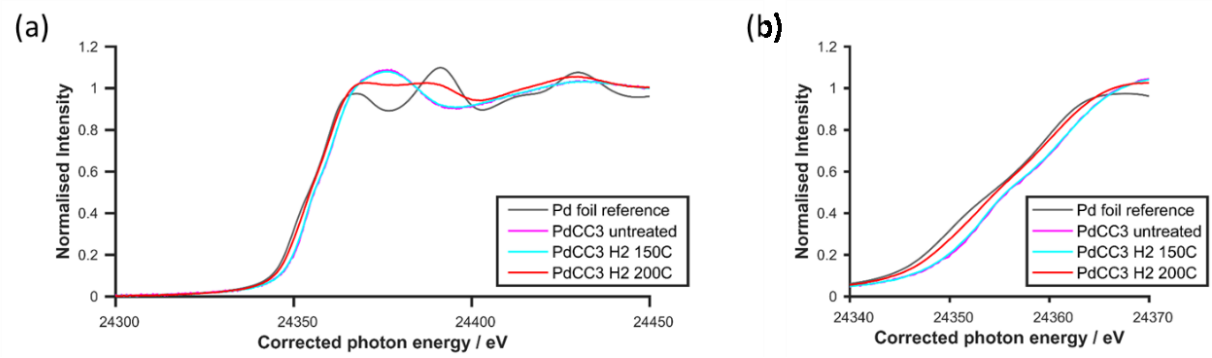

Figure S6. Normalised XANES spectra (a) near and (b) expanded (as in main text) at the Pd K-edge for Pd reference foil, **Pd(NO$_3$)$_2$@CC3** before reduction and after reduction in 10% H_2 at 150 °C and 200 °C (**Pd NPs@CC3**). The photon energy scale has been corrected by alignment of concurrently measured Pd foil data.

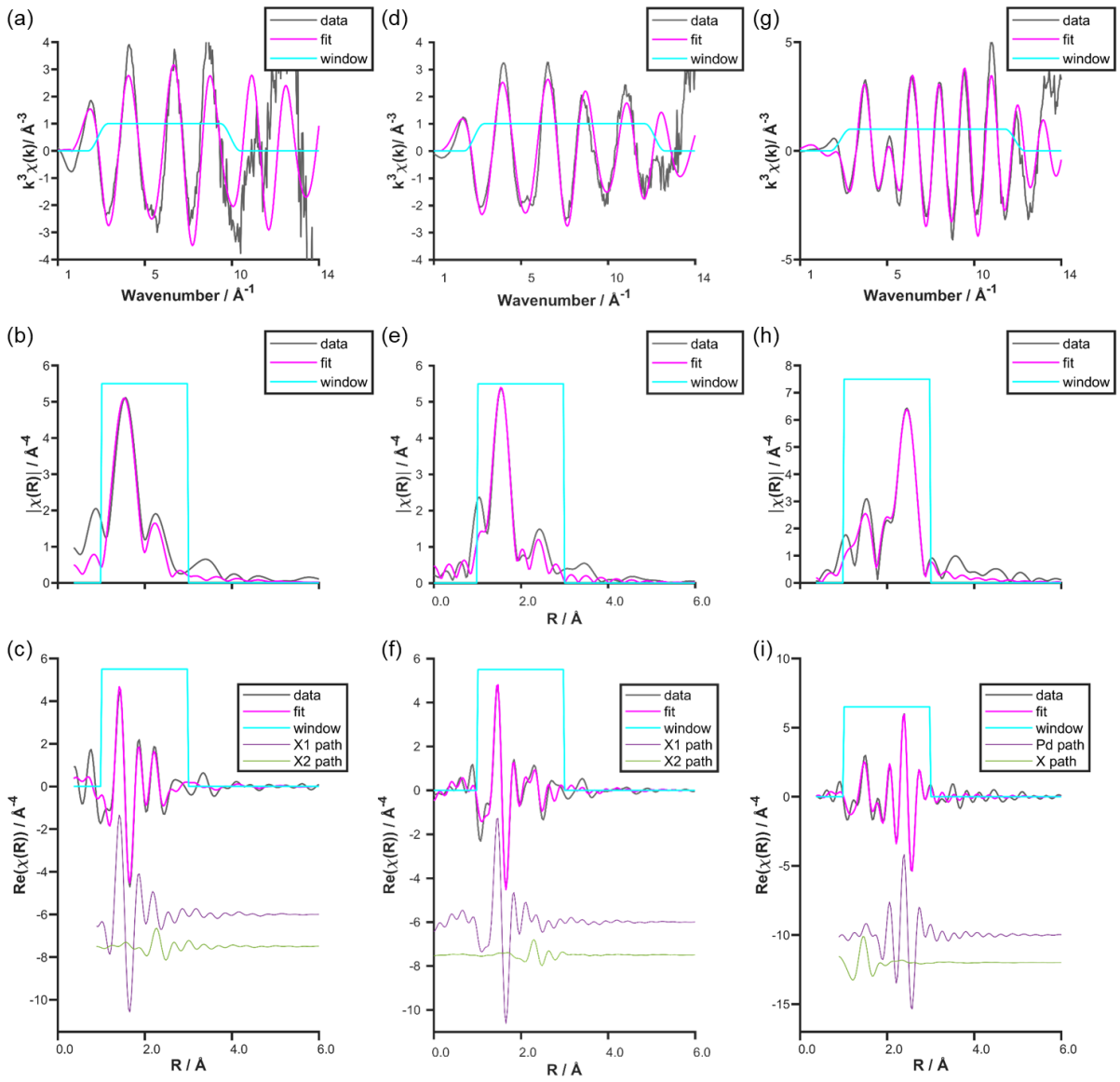

Figure S7. EXAFS spectroscopy data and first shell fits of **$Pd(NO_3)_2$@CC3** untreated (left), after H_2 reduction at 150 °C (middle) and **Pd NPs@CC3** formed after H_2 reduction at 200 °C (right), showing (a, d, g) k-space and (b,e,h) magnitude R-space fits, along with (c,f,i) the real part of the R-space fit and component path contributions used listed in order of increasing effective R-distance. Fit parameters and information shown in Table S4.

Table S4. EXAFS fitting parameters for the Pd K-Edge plots shown in Figure S6.[a]

refined parameter	**$Pd(NO_3)_2$@CC3**	**$Pd(NO_3)_2$@CC3** after H_2 150 °C	**Pd NPs@CC3** (after H_2 200 °C)
ΔE_0	11(3)	7(2)	-7.6(9)
CN_{Pd-Pd}	†	†	5.1(7)
CN_{Pd-X1}	2.8(7)	3.0(5)	2.5(1.0)
CN_{Pd-X2}	1.5(1.1)	1.3(8)	†
R_{Pd}	†	†	2.738(07)
R_{X1}	2.015(4)	2.014(14)	1.974(16)
R_{X2}	2.85(5)	2.85(6)	†
σ^2_{Pd}	†	†	0.009(1)
σ^2_X	0.002(3)	0.003(2)	0.010(5)
goodness of fit			
R-factor	0.04	0.04	0.02
fitting range			
k-range	3.0 – 9.6	3.0 – 12.0	3.0 – 11.7
R-range	1.0 – 3.0	1.0 – 3.0	1.0 – 3.0
No. of independent points	8	11	11
No. of fitted parameters	6	6	7

[a]Fitting parameters: S_0^2 = 0.87 as determined by the use of a Pd foil standard; X1 and X2 denote small heteroatoms at two fixed co-ordination distances, based initially on the nearest neighbour oxygen and nitrogen in $Pd(NO_3)_2$; σ^2_X is taken to be the mean-squared relative deviation for both X1 and X2. Parameters marked † belong to components producing a less good or unphysical fit when included, indicating they do not contribute significantly to the spectra (in the case of Pd-X2, this component did not contribute significantly to PdCC3 H_2 200 °C because it is overwhelmed by the strength of the Pd-Pd interaction, but the lack of a fit for them doesn't imply they are not physically present).

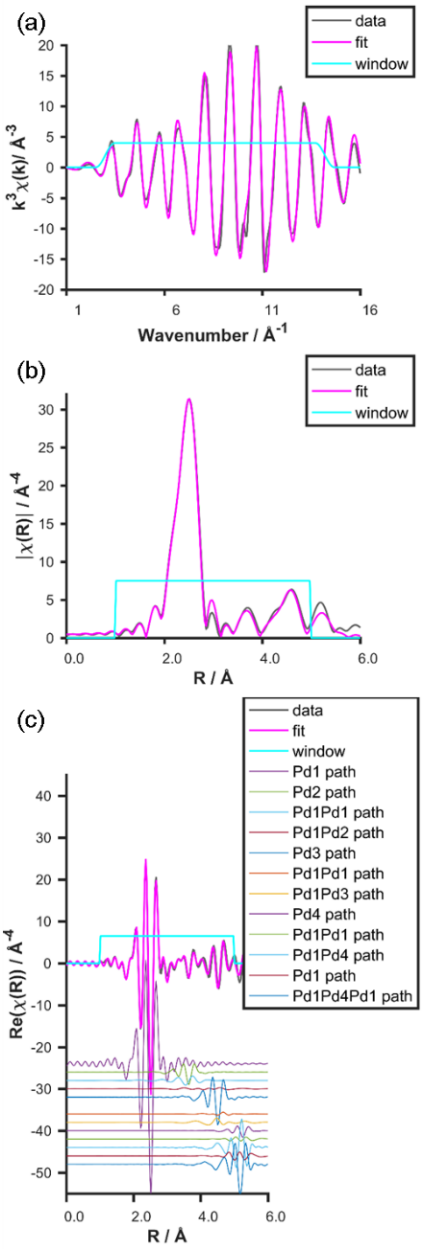

Figure S8. Fit to extended R space region for Pd foil reference used to determine S_0^2, showing (a)k-space and (b) magnitude R-space fits, along with (c) the real part of the R-space fit and component path contributions listed in order of increasing effective R-distance. Fit parameters and information shown in Table S5. As discussed in the methods section, the extended fit was conducted to improve the reliability for the two metallic fits to account for multiple scattering and longer paths.

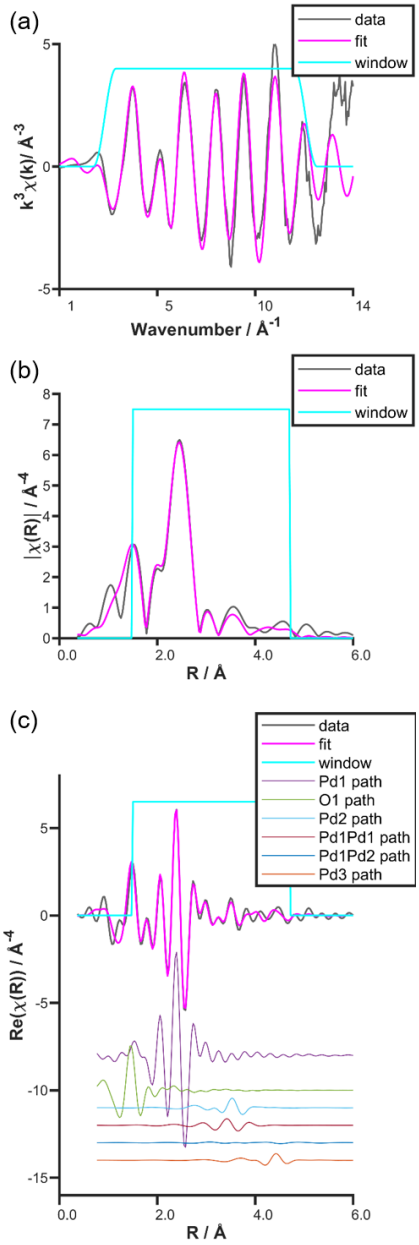

Figure S9. Fit to extended R space region for PdCC3 H_2 200 °C, showing (a) k-space and (b) magnitude R-space fits, along with (c) the real part of the R-space fit and component path contributions listed in order of increasing effective R-distance. Fit parameters and information shown in Table S5. As discussed in the methods section, the extended fit was conducted to improve the reliability for the two metallic fits to account for multiple scattering and longer paths.

Table S5. Fit to extended R space region for PdCC3 H_2 200 °C and Pd metal corresponding to Figures S8 and S9.[a] As discussed in the methods section, the extended fit was conducted to improve the reliability for the two metallic fits to account for multiple scattering and longer paths.

refined parameter	PdCC3 H_2 200 °C	Pd metal foil
S_0^2	Fixed @ 0.87	0.87(4)
ΔE_0	-8.0(7)	3.8(3)
Pd lattice expansion factor	-0.0051(19)	-0.0027(7)
σ^2_{Pd1}	0.0092(9)	0.0058(3)
σ^2_{Pd2}	0.020(11)	0.0097(17)
σ^2_{Pd3}	0.024(15)	0.0096(08)
σ^2_{Pd4}	Not included [b]	0.011(3)
σ^2_X	0.006(4)	Not included [c]
RX	1.969(14)	Not included [c]
CN_X	2.4(0.8)	Not included [c]
CN_{Pd1}	5.3(6)	Fixed = 12
CN_{Pd2}	4.8(4.5)	Fixed = 6
CN_{Pd3}	10(9)	Fixed = 24
$CN_{Pd1xPd1}$	35(20)	Fixed = 48
goodness of fit		
R-factor	0.01	0.01
fitting range		
k-range	3.0 – 11.9	3.0 – 14.2
R-range	1.5 – 4.7	1.0 – 5.0
No. of independent points	18	28
No. of fitted parameters	12	7

[a]Fitting parameters: $S_0^2 = 0.87$ was used for the PdCC3 H_2 200 °C sample as determined by the use of a Pd foil standard; X denotes a small heteroatom at fixed co-ordination distance R_X, based initially on the nearest neighbour oxygen in $Pd(NO_3)_2$. [b]A fourth shell Pd contribution was not included as significantly outside the R-range employed in the fit. [c]The heteroatom contribution was not included in the fit to the pure metal foil as there should not be significant oxidation in the bulk material.

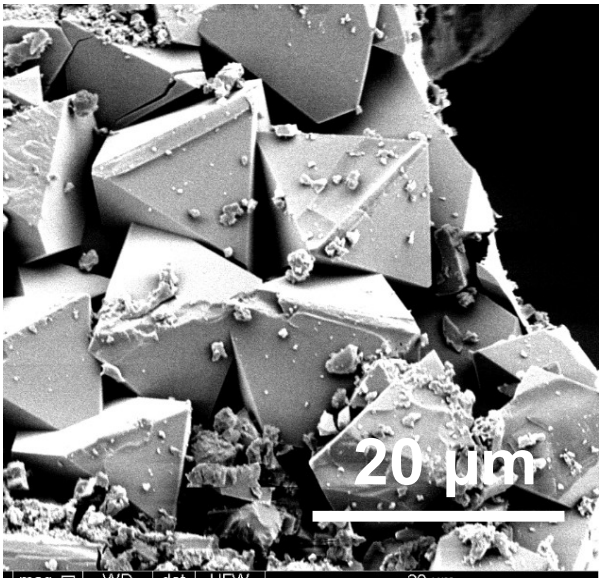

Figure S10. SEM image of 0.5 wt.% **Pd NPs@CC3** showing octahedral shaped crystals.

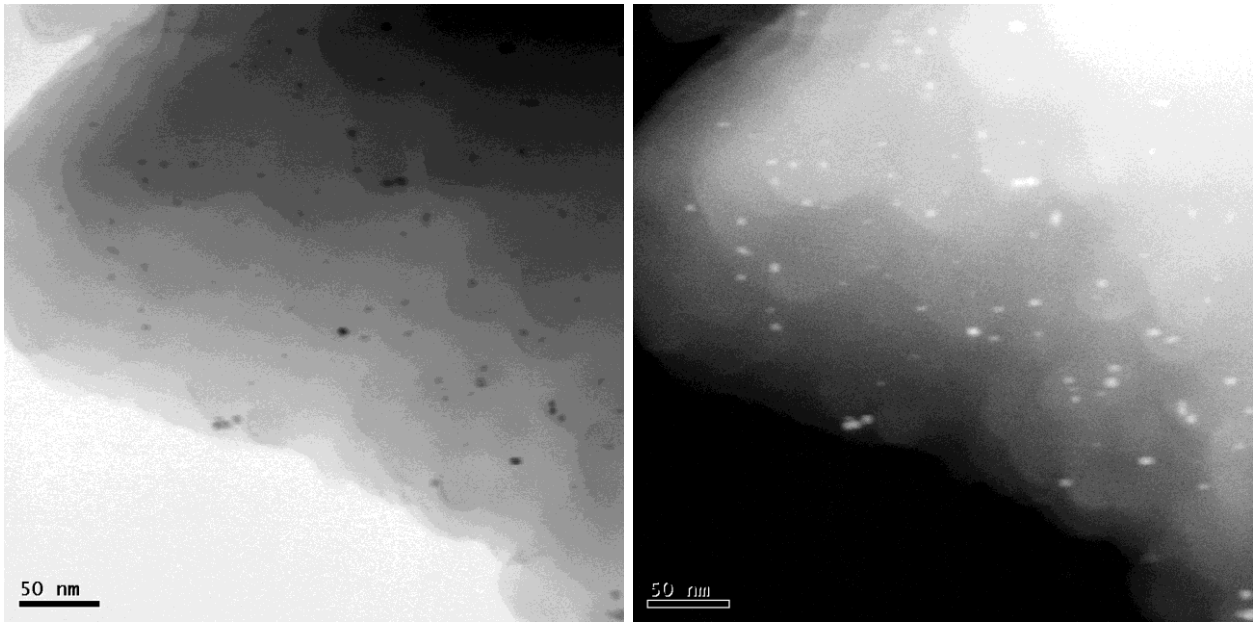

Figure S11. Bright field (left) and dark field (right) STEM images of 1 wt.% Pd NP@**CC3** catalyst to show small NPs embedded into **CC3** for a higher loading sample than those shown in main text.

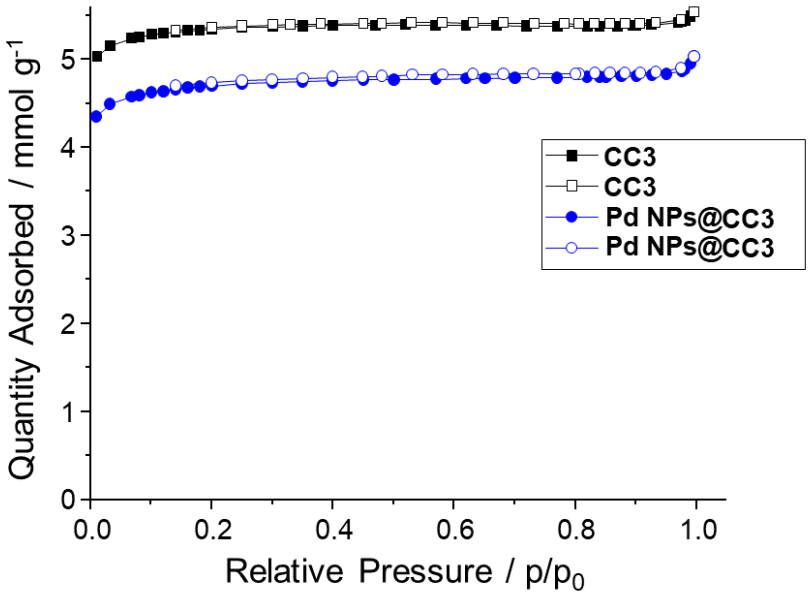

Figure S12. Nitrogen adsorption (solid symbols) and desorption (open symbols) at 77 K for **CC3** (black) and the 0.5 wt.% **Pd NPs@CC3** (blue).

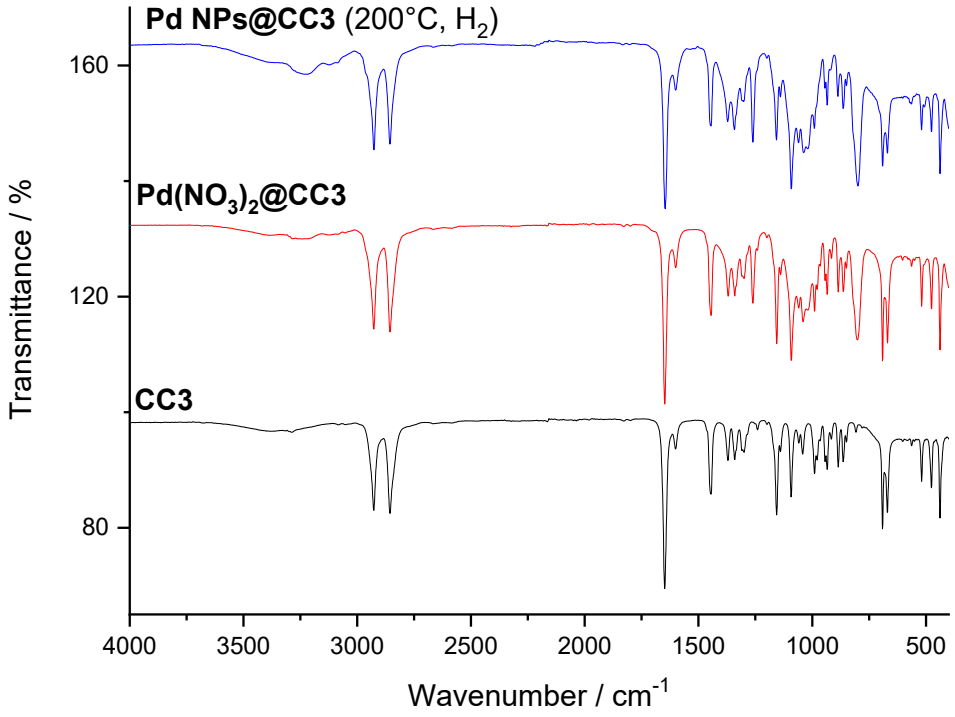

Figure 13. FTIR spectra for **CC3** (black), 2 wt.% **Pd(NO$_3$)$_2$@CC3** (red), and 2 wt.% **Pd NPs@CC3** after H_2 reduction at 200 ˚C for 1 hour (blue). Note a higher loading was used in this case to ensure any differences should be more pronounced in the resulting spectra.

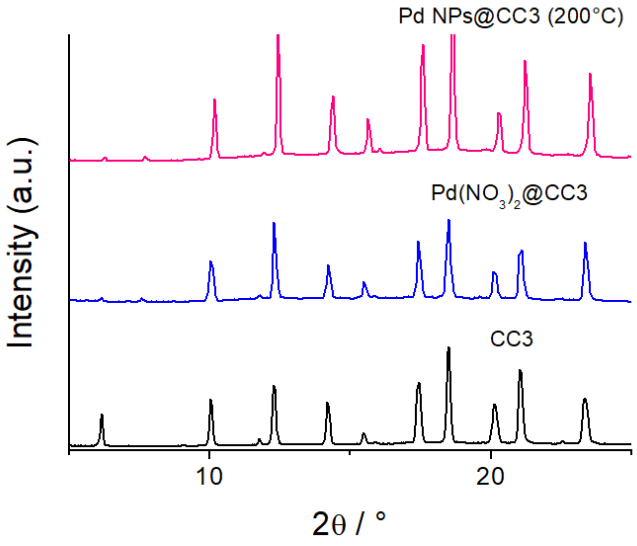

Figure S14. An enlarged view of PXRD patterns (main text Figure 4) of **CC3** (black), desolvated 0.5 wt.% **Pd(NO$_3$)$_2$@CC3** (blue) and 0.5 wt.% **Pd NPs@CC3** after H_2 reduction at 200 ˚C (pink). The features at 7.6 °, 11 ° and 19.5 ° in both 0.5 wt.% **Pd(NO$_3$)$_2$@CC3** and 0.5 wt.% **Pd NPs@CC3** after H_2 reduction could be due to a minor *R3* second polymorph.

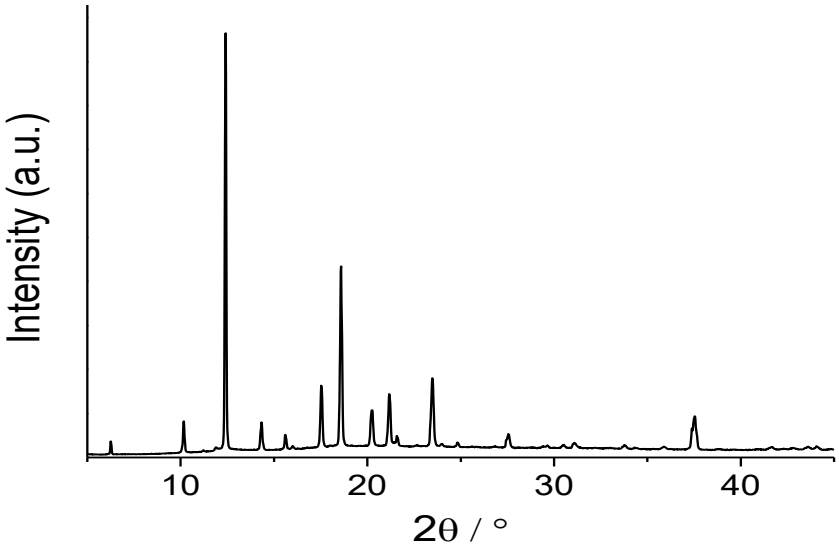

Figure S15. PXRD of pure CC3 re-crystallized from DCM / acetone without Pd(NO$_3$)$_2$ under conditions corresponding to those used when Pd(NO$_3$)$_2$ is added, confirming the additional reflections seen with Pd(NO$_3$)$_2$ are not due to the DCM/acetone mixture (10 mg CC3 recrystallized from 2 mL DCM and 500 µL acetone).

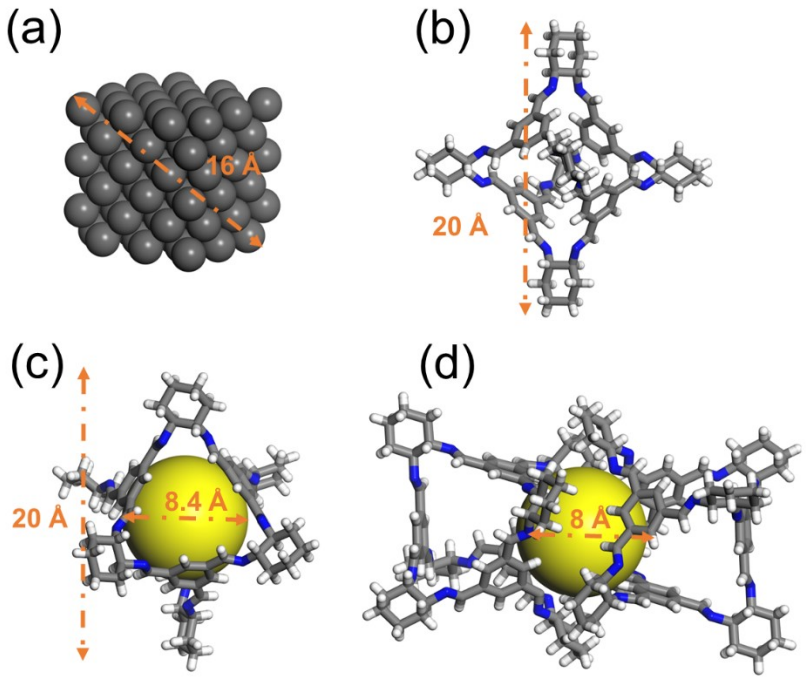

Figure S16. (a) The Pd_{104} cluster model to represent the average nanoparticle size of 1.6 nm; (b) the size of cage molecule is 20 Å indicating the overall size of **CC3** molecule (rather than the internal cage) is comparable to Pd NPs; (c) the internal cavity of a cage is 8.4 Å in diameter; (d) the pore cavity between a pair of cage molecules is 8 Å.

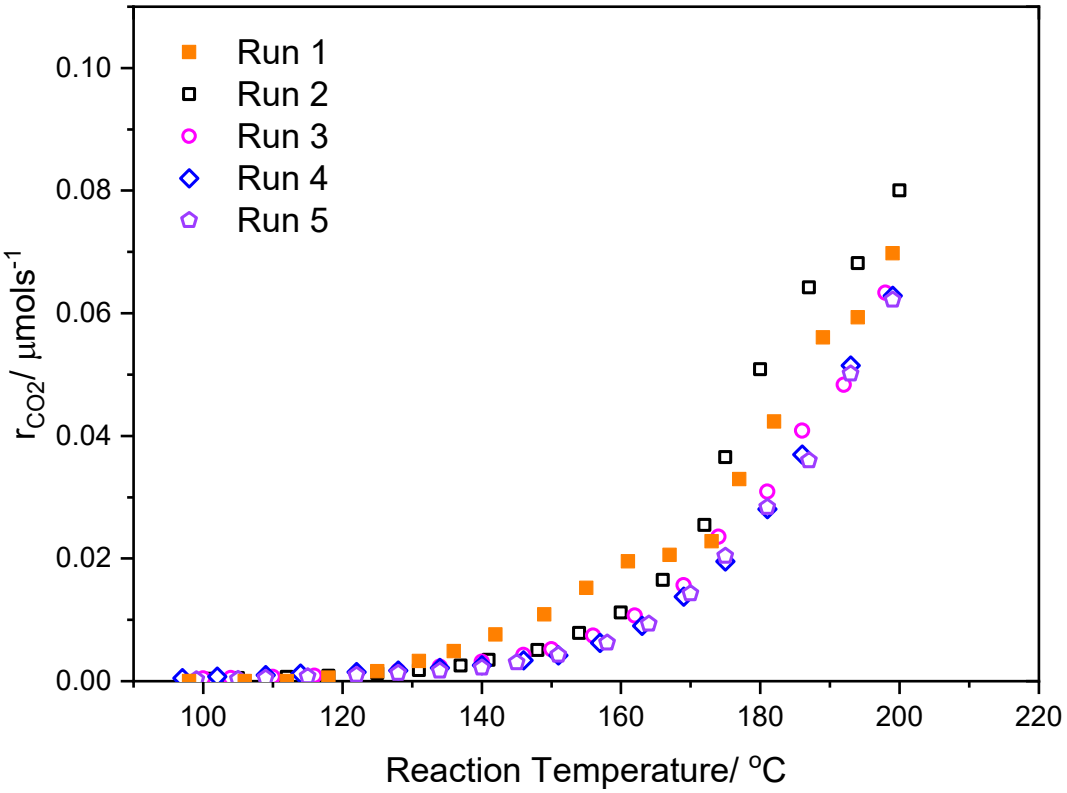

Figure S17. Repeat cycling of the catalyst as a function of temperature showing little change in the measured conversion (3% CO, 15% O_2, balance He, total flow 60 mLmin^{-1}; ambient pressure; 71.5 mg of 0.5 wt.% Pd catalyst). Note, the first run was conducted under a slightly higher CO:O_2 ratio, and has been corrected by a known partial pressure dependence).

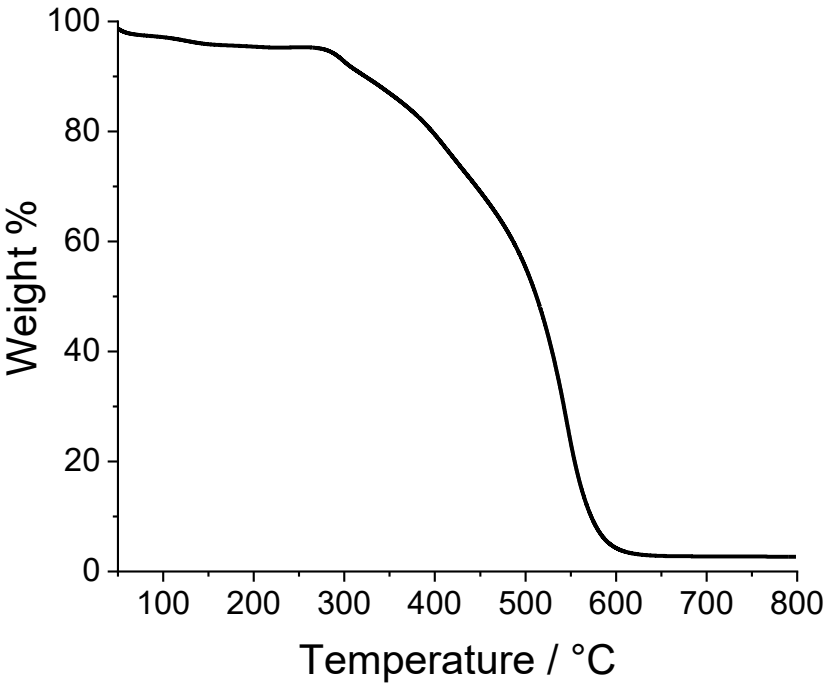

Figure S18. TGA mass loss profile of 0.5 wt.% **Pd NPs@CC3** under air flow.

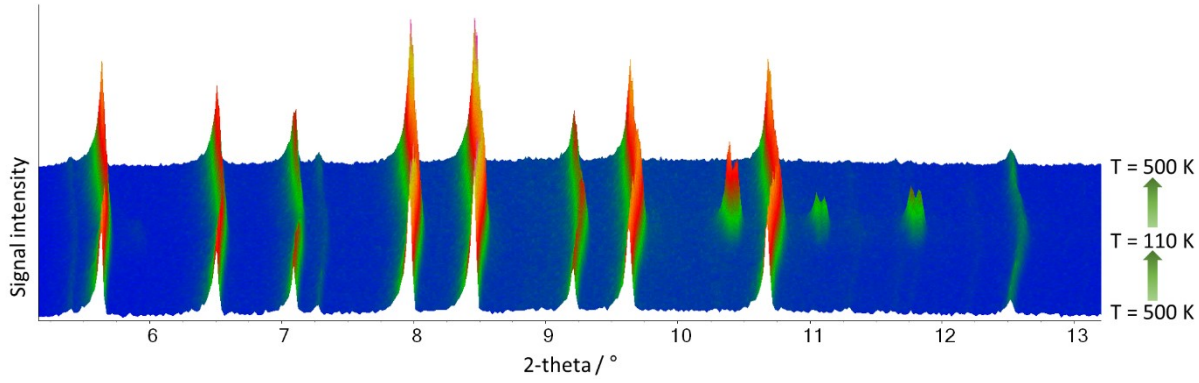

Figure S19. VT-PXRD study of 0.5 wt.% **Pd NPs@CC3** to determine the structural stability in the temperature range between 110 K and 500 K. All additional reflections seen at low temperature are due to diffraction by ice on the sample holder.

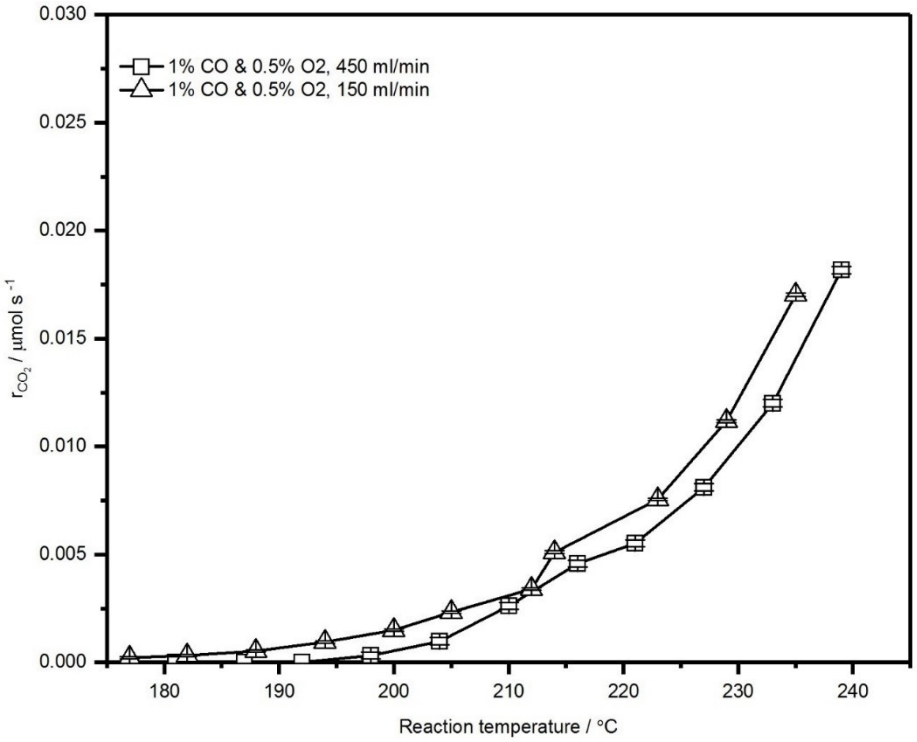

Figure S20. Light off data for a similar catalyst under higher flow rate conditions (150 $mLmin^{-1}$ and 450 $mLmin^{-1}$ as compared to 60 $mLmin^{-1}$ used for data shown in main text; 1% CO, 0.5% O_2, balance He; ambient pressure), confirming the mass transfer effects along the reactor bed are minimal.

References

1. Newville, M., IFEFFIT : interactive XAFS analysis and FEFF fitting. *Journal of Synchrotron Radiation* **2001,** *8* (2), 322-324.
2. Ravel, B.; Newville, M., ATHENA, ARTEMIS, HEPHAESTUS: data analysis for X-ray absorption spectroscopy using IFEFFIT. *Journal of Synchrotron Radiation* **2005,** *12* (4), 537-541.
3. Bruns, J.; Klüner, T.; Wickleder, M. S., Oxoanionic Noble Metal Compounds from Fuming Nitric Acid: The Palladium Examples Pd(NO3)2 and Pd(CH3SO3)2. *Chemistry – A European Journal* **2015,** *21* (3), 1294-1301.